

# Communication Analysis and Optimization of 3D Front Tracking Method for Multiphase Flow Simulations

Journal Title  
XX(X):1–12  
©The Author(s) 0000  
Reprints and permission:  
sagepub.co.uk/journalsPermissions.nav  
DOI: 10.1177/ToBeAssigned  
www.sagepub.com/  


Muhammad Nufail Farooqi<sup>1</sup>, Daulet Izbassarov<sup>2</sup>, Metin Muradoğlu<sup>2</sup> and Didem Unat<sup>1</sup>

## Abstract

This paper presents scalable parallelization of an Eulerian-Lagrangian method, namely 3D front tracking method, for simulating multiphase flows. Operating on Eulerian-Lagrangian grids makes the front tracking method challenging to parallelize and optimize because different types of communication (Lagrangian-Eulerian, Eulerian-Eulerian and Lagrangian-Lagrangian) should be managed. In this work, we optimize the data movement in both the Eulerian and Lagrangian grids and propose two different strategies for handling the Lagrangian grid shared by multiple subdomains. Moreover, we model three different types of communication emerged as a result of parallelization and implement various latency-hiding optimizations to reduce the communication overhead. Good scalability of the parallelization strategies are demonstrated on two supercomputers. Strong scaling study using 256 cores simulating 1728 interfaces or bubbles achieves 32.5x speedup. We also conduct weak scaling study on 4096 cores simulating 27648 bubbles on a  $1024 \times 1024 \times 2048$  Eulerian grid resolution.

## Keywords

Front Tracking Method, Direct Numerical Simulation, Multiphase Flow, Communication Optimization

## Introduction

Computational simulation of multiphase flows is crucial for understanding many industrial processes and natural phenomena [1, 2]. In the simulation of multiphase flows an interface, called *front* separates different fluids. The treatment of the front poses great difficulty because it continuously evolves, deforms and even undergoes topological changes. Various discretization techniques have been developed for treating a front (see Tryggvason et al. [3] for an overview). Two of the most popular techniques discussed in Tryggvason et al. [3] are front tracking, where the front is explicitly tracked using a Lagrangian grid (Eulerian-Lagrangian approach) and front capturing method, where the front is implicitly represented in an Eulerian grid (Eulerian-Eulerian approach). For accurate as well as stable simulations both front capturing and front tracking methods need a high spatial and temporal resolution, which in turn demands high computational power. To keep computational time within practical limits simulations are needed to be done in parallel.

The literature presents many studies on the parallelization of single-phase flow simulations [4, 5]. Most of the existing parallel implementations [9, 8, 10, 7] have focused on the front capturing methods such as volume-of-fluid (VOF), level-set and phase-field methods because they are similar to the common single-phase flow solvers that use Eulerian methods.

The front tracking method is advantageous as it preserves mass very well, virtually eliminates numerical diffusion of interface (i.e., the interface thickness remains the same), and calculates the interfacial physics accurately. However, the Eulerian-Lagrangian methods (e.g., front tracking method) compared to the Eulerian-Eulerian methods are more

challenging to parallelize because in addition to the Eulerian grid, the Lagrangian grid and communication between the two grids should be handled in the computation.

With the current technology trends, communication cost between processors exceeds computation cost both in terms of energy consumption and performance [41, 42]. For scalability on modern architectures, large-scale applications such as multiphase flow simulations have to optimize their data movement using communication hiding and avoiding techniques [24, 25, 26]. In this paper, we study a 3D front tracking method and optimize the communication both in Eulerian and Lagrangian grids using MPI for modern large-scale parallel architectures. The Lagrangian grid (e.g. bubble) is unstructured, movable, and continuously restructured with time, which poses great difficulties in its parallelization. To handle the communication between Lagrangian grids, we design two parallelization strategies: *owner-computes* and *redundantly-all compute*. The *owner-computes* associates a shared Lagrangian grid with a single processor and communicates the newly computed data with the sharers. The *redundantly-all compute* strategy adopts a different approach, where the shared Lagrangian grid is computed by all the sharers at the expense of increased computation but reduced communication. We implement

<sup>1</sup>Department of Computer Engineering, Koc University, Rumelifeneri Yolu, 34450 Sariyer, Istanbul, Turkey.

<sup>2</sup>Department of Mechanical Engineering, Koc University, Rumelifeneri Yolu, 34450 Sariyer, Istanbul, Turkey.

## Corresponding author:

Didem Unat. Tel.: +90 (212) 338 1583; fax: +90 (212) 338 15 48.

Email: dunat@ku.edu.tr

both strategies and explore their actual performance on two supercomputers.

Our contributions can be summarized as follows:

- We analyze and optimize the parallelization of both the Eulerian and Lagrangian grids for a three-dimensional front tracking method.
- We develop two parallelization strategies for Lagrangian grids: *owner computes* and *redundantly all compute*, and compare their resulting communication cost by modeling three different types of communication (Lagrangian-Eulerian, Eulerian - Eulerian and Lagrangian - Lagrangian).
- By using realistic problem settings, we conduct strong scaling study using 256 cores simulating 1728 bubbles and achieve 32.5x speedup over the baseline. We also perform weak scaling study up to 4096 cores simulating 27648 bubbles and observe good scalability.

The rest of the paper is organized as follows: In the next section, we present the related work. Then we briefly describe the formulation and numerical algorithm behind the front tracking method. Next, we develop a data dependency graph among different tasks of the front tracking method and provide details of parallelization strategies. Then we present and compare models for different types of communication used in the front tracking method. After that, we discuss the implementation details for parallelization, and provide the results for strong and weak scaling of the parallelized code. Finally, we draw conclusions.

## Related Work

In the literature, efforts towards the performance studies of parallel Eulerian-Lagrangian methods are limited either to a small number of processors or to a small number of bubbles (interfaces). The early idea of the front tracking method has been mainly developed by Glimm and coworkers [14, 15]. In their version of front tracking, the interface itself is described by additional computational elements and the evolving interface is represented by a connected set of points forming a moving internal boundary. An irregular grid is then constructed in the vicinity of the interface and a special finite-difference stencil is used to solve the flow equations on this irregular grid. Glimm's implementation is available as the FronTier library [16, 17, 18]. Later, Tryggvason and coworkers [19, 20] improved the front-tracking method so that the fixed grid does not change near the interface. Moreover, unlike the Glimm's front tracking method, where different phases are treated separately, in Tryggvason's method different phases are treated as a single phase, which makes simulating many bubble cases easier. In the present study, we base our implementation on the version of the front tracking method developed by Unverdi and Tryggvason [19]. Esmaceli and Tryggvason [21] and Bunner and Tryggvason [22, 23] studied the motion of a few hundred two-dimensional and three-dimensional bubbles, respectively, using the front tracking method. Bunner et al. [6] parallelized the front tracking method on 3D Eulerian grid using domain decomposition and the Lagrangian grid was parallelized using a master-slave approach. The

Lagrangian grid shared by multiple subdomains is computed by the master process in the master-slave approach. The master process also distributes the updated data to the slave processes.

In an Eulerian-Lagrangian multiphase flow simulation, particles can be used to represent phases. They can be connected if they are used to separate the phases or they can be independent, representing different phases. Existing Eulerian-Lagrangian methods usually use independent particles, which are easier to parallelize compared to connected ones. In the connected particle cases as in the front tracking method, coupled data between the Eulerian and Lagrangian grids makes it more challenging to parallelize. For example, Darmana et al. [12] and Nkonga and Charrier [11] parallelized the independent particles using a domain decomposition method for both Eulerian and Lagrangian grids.

Kuan et al. [13] parallelized the connected particle Eulerian-Lagrangian method by applying domain decomposition to both grids. They spatially decompose the Lagrangian grid similar to the Eulerian grid. They overlap the subdomains during decomposition to hide communication with computation and perform re-decomposition each time the Lagrangian marker points move out of the subdomain. To keep track of subparts of the Lagrangian grid they carry out some extra computation for grid's connectivity construction. Although they use one or two interfaces in their simulations, the implementation achieves only modest scaling on small number of processors.

The main focus of the prior work about the parallelization of the Eulerian-Lagrangian methods for multiphase flows by [11, 12, 13] relied on domain decomposition and focused less on the resulting communication overhead. In this work, we model the resulting communication in depth and implement two strategies for the Eulerian-Lagrangian method. The increasing gap between the computational and communication capabilities have forced researchers to look for techniques to deal with the architectural limitations. Redesigning of algorithms to avoid or hide communication by replicating the computation is becoming an alternative technique to deal with the rising gap. Some of the motivational work inspiring our methods are based on communication avoiding algorithms developed by Demmel [24] for direct and iterative linear algebra, Demmel et al. [25] for support vector machines on distributed memory systems and Yelick et al. [26] for N-body particle interactions algorithm.

## Front Tracking Method

The governing equations are described in the context of the finite difference or front tracking method [20]. The flow is assumed to be incompressible. Following Unverdi and Tryggvason [19], a single set of governing equations can be written for the entire computational domain provided that the jumps in the material properties such as density and viscosity are taken into account and the effects of the interfacial surface tension are treated appropriately.

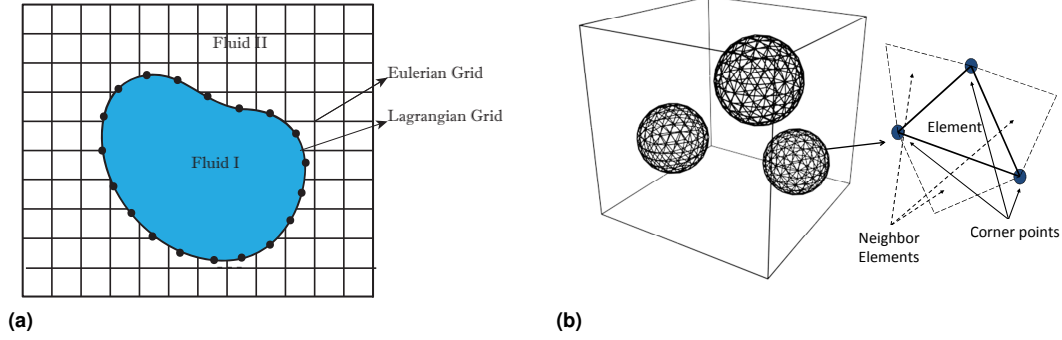


**Figure 1.** (a) Lagrangian and Eulerian grids in 2D. The flow equations are solved on the fixed Eulerian grid. The interface between different phases is represented by a Lagrangian grid consisting of connected Lagrangian points (marker points). (b) Structure of a 3D interface. Each interface is a collection of triangular elements, which have pointers to the marker points and to the adjacent elements. Marker points are the corner points of an element.

The continuity and momentum equations can be written as follows:

$$\begin{aligned} \nabla \cdot \mathbf{u} &= 0, \\ \rho \frac{\partial \mathbf{u}}{\partial t} + \rho \nabla \cdot (\mathbf{u} \mathbf{u}) &= -\nabla p + \nabla \cdot \mu (\nabla \mathbf{u} + \nabla^T \mathbf{u}) \\ &+ \Delta \rho \mathbf{g} + \int_A \sigma \kappa \mathbf{n} \delta(\mathbf{x} - \mathbf{x}_f) dA, \end{aligned} \quad (1)$$

where  $\mu$ ,  $\rho$ ,  $g$ ,  $p$  and  $\mathbf{u}$  denote the viscosity and the density of the fluid, the gravitational acceleration, the pressure and the velocity vector, respectively. The last term in Eq. (2) represents the body force due to surface tension where  $\sigma$  is the surface tension coefficient,  $\kappa$  is twice the mean curvature, and  $\mathbf{n}$  is the unit vector normal to the interface, respectively. The surface tension acts only on the interface as indicated by the three-dimensional delta function,  $\delta$ , whose arguments  $\mathbf{x}$  and  $\mathbf{x}_f$  are the points at which the equation is evaluated and a point at the interface, respectively.

It is also assumed that the material properties remain constant following a fluid particle, i.e.,

$$\frac{D\rho}{Dt} = 0; \quad \frac{D\mu}{Dt} = 0; \quad (3)$$

where  $\frac{D}{Dt} = \frac{\partial}{\partial t} + \mathbf{u} \cdot \nabla$  is the material derivative. The density and viscosity vary discontinuously across the fluid interface and are given by

$$\mu = \mu_i I + \mu_o(1 - I); \quad \rho = \rho_i I + \rho_o(1 - I); \quad (4)$$

where the subscripts  $i$  and  $o$  denote the properties of the drop and bulk fluids, respectively, and  $I$  is the indicator function defined such that it is unity inside the droplet and zero outside.

The flow equations (Eqs. 1-2) are solved on a stationary staggered Eulerian grid. The spatial derivatives are approximated using second order central finite-differences for all field quantities except for the convective terms that are discretized using a third order QUICK scheme [27]. The time integration is achieved using a projection method first proposed by Chorin [28]. The numerical method is briefly described here in the framework of the actual FORTRAN implementation. The method is explicit so the time step

$\Delta t$  is restricted for numerical stability and computed at the beginning of the time stepping loop as

$$\Delta t = \alpha_{sf} \min \left( \frac{h_{min}^2}{6s_{max}}, \left( \frac{h}{U} \right)_{min} \right), \quad (5)$$

where  $s_{max}$  is the largest value among the kinematic viscosities of the drop and ambient fluids and  $h_{min}$  is the smallest grid size.  $(h/U)_{min}$  is the minimum value of grid size  $h$  divided by the magnitude of velocity  $U$  in the domain, and  $\alpha_{sf}$  is the safety factor taken as 0.9 in this study. Then the increment in velocity vector due to the convection and viscous terms is computed using the quantities evaluated at the previous time level  $n$  as

$$d\mathbf{u} = \left[ \nabla \cdot (\mathbf{u} \mathbf{u}) + \frac{\nabla \cdot \mu (\nabla \mathbf{u} + \nabla^T \mathbf{u})}{\rho} \right]^n, \quad (6)$$

where the convective terms are evaluated using the QUICK scheme [27] while the viscous terms are approximated using the central differences on the staggered grid. The body force due to surface tension forces is evaluated as

$$\mathbf{f}_f = \left[ \int_A \sigma \kappa \mathbf{n} \delta(\mathbf{x} - \mathbf{x}_f) dA \right]^n, \quad (7)$$

where it is first computed on the Lagrangian grid and is then distributed onto the neighboring Eulerian grid using the Peskin's cosine distribution function as discussed in detail by Tryggvason et al. [20]. The front is then moved by a single time step using an explicit Euler methods as

$$\mathbf{x}_f^{n+1} = \mathbf{x}_f^n + \mathbf{u}_f^n \Delta t, \quad (8)$$

where  $\mathbf{u}_f^n$  is the velocity interpolated onto the location of the marker point from the Eulerian grid. After this step, the body force due to surface tension forces is added to the buoyancy force and  $d\mathbf{u}$ . Then the unprojected velocity field  $\mathbf{u}^*$  is computed as

$$d\mathbf{u} = d\mathbf{u} + \frac{\mathbf{g} \Delta \rho^n}{\rho^n} + \frac{\mathbf{f}_f}{\rho^n}, \quad (9)$$

$$\mathbf{u}^* = \mathbf{u}^n + \Delta t d\mathbf{u}. \quad (10)$$

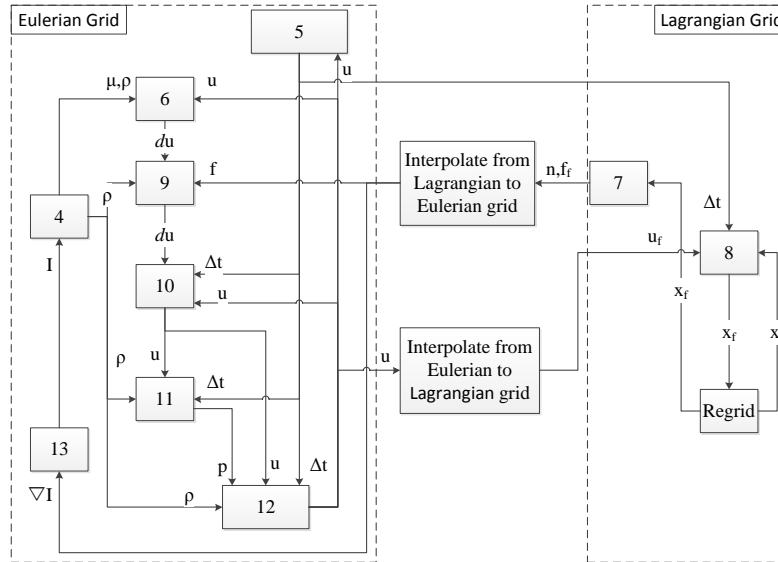


**Figure 2.** Data dependency among tasks in front tracking method (number inside the rectangle indicates the equation number computed in that task).

To enforce the incompressibility condition, the pressure field is computed by solving a Poisson equation in the form

$$\nabla \cdot \left( \frac{1}{\rho^n} \nabla p^{n+1} \right) = \frac{1}{\Delta t} \nabla \cdot \mathbf{u}^*. \quad (11)$$

The Poisson equation (Eq. 11) is solved for the pressure using the HYPRE library [35]. Then the velocity field is corrected to satisfy the incompressibility condition as

$$\mathbf{u}^{n+1} = \mathbf{u}^* - \frac{\Delta t}{\rho^n} \nabla p^{n+1}. \quad (12)$$

Finally the indicator function is computed using the standard procedure as described by Tryggvason et al. [20], which requires solution of a separable Poisson equation in the form

$$\nabla^2 I^{n+1} = \nabla \cdot (\nabla I)^{n+1}, \quad (13)$$

which is again solved using the HYPRE library [35]. To evaluate the right hand side of Eq. 13, unit normal vectors are first computed at the center of each front element, then distributed onto neighboring Eulerian grid points in a conservative manner, and finally the divergence is evaluated using central differences.

The numerical methods describe above is first order accurate in time. However, second-order accuracy is recovered by using a simple predictor-corrector scheme in which the first-order solution at  $n + 1$  serves as a predictor that is then corrected by the trapezoidal rule as discussed by Tryggvason et al. [20].

In the front tracking method, the interface is used to explicitly track the fluid-fluid interface as shown in Fig 1a. The interface consists of Lagrangian points (or marker points) connected by triangular elements as shown in Fig 1b. The Lagrangian points are used to compute the surface tension forces on the interface, which are then distributed as body forces using the Peskin's cosine distribution function [29] over the neighboring Eulerian grid cells [19, 20]. The indicator function is computed at each timestep based on the location of the interface using the

standard procedure [19, 20] and is then used to set the fluid properties in each phase according to Eq. 4. The restructuring is performed by deleting the elements that are smaller than a pre-specified lower limit and by splitting the elements that are larger than a pre-specified upper limit in the same way as described by Tryggvason et al. [20] to keep the element size nearly uniform. It is critically important to restructure the Lagrangian grid since it avoids unresolved wiggles due to small elements and lack of resolution due to large elements.

More details about the front tracking method can be found in the original paper by Unverdi and Tryggvason [19], the review paper by Tryggvason et al. [20] and the recent book by Tryggvason et al. [3]. For different applications of the method, see [30, 31, 32, 33, 34].

## Parallelization of the Front Tracking Method

In this section we present the parallelization method used for the front tracking method, particularly focus on the parallelization of the Lagrangian grid. We first derive a data dependency graph for the equations as shown in Fig 2. A grey rectangle in the figure represents a task and the number inside a task indicates which equation it solves. The arrows indicate data dependencies from one task (equation) to another. As Fig 2 suggests all tasks are dependent on the data from other tasks. However, the computations on the Eulerian and Lagrangian grids can be performed in parallel.

We refer the processes computing on the Eulerian grid as *Domain* processes and the processes computing on the Lagrangian grid as *Front*. The Eulerian grid is a structured grid as a result simple domain decomposition can be easily applied for its parallelization. Each subdomain can be assigned to one MPI-process. Similar to the Eulerian grid, we subdivide the Lagrangian grids into subgrids, and distribute bubbles among parallel *Fronts*. The *Front*, which contains the center of a bubble becomes the owner of that bubble. Each *Front* is mapped to a number of *Domain* processes and the *Front* communicates with only these *Domains*. An example mapping of 8 *Domains* to 2 *Fronts* is shown in Fig 3a.

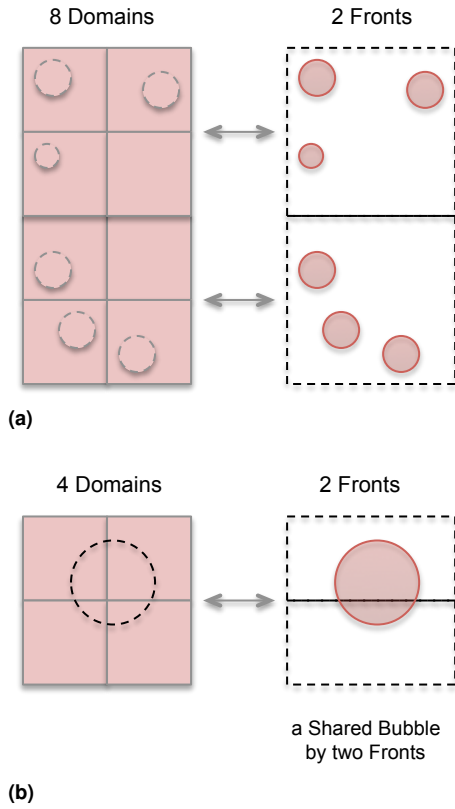


**Figure 3.** (a) Work division for parallel *Fronts* where upper 4 *Domains* are assigned to upper *Front* and lower 4 *Domains* are assigned to lower *Front*. (b) Two parallel *Fronts* with a shared bubble.

A bubble may move anywhere in the physical domain over time. There is a possibility that a bubble may be lying at the border and shared by more than one *Front* as shown in Fig 3b, where a single bubble is shared by 2 *Fronts*. Shared bubbles complicate parallelization. To update the coordinates of the marker points that do not lie inside the owner *Front* are needed to be sent and received to or from other *Fronts*. One approach to deal with such bubbles is to break the bubble into parts and each *Front* works only on its own portion as discussed by Bunner [6]. This approach is computationally much more complex as it requires matching points and elements at the boundaries to maintain the data coherency. Instead we propose the following two approaches:

- **Owner-Computes:** In this approach, the shared bubble is computed by the owner *Front*, which contains the center of the bubble and updates the sharers. The responsibilities of the owner include solving the equations, keeping track of the sharers, sending or receiving the data ( $n$ ,  $f_f$ , and  $x_f$ ) associated with shared portion of the bubble to or from corresponding sharers. The responsibility of sharers is only to route the shared data of the bubble to the corresponding *Domains*.
- **Redundantly-All-Compute:** This strategy eliminates the communication of  $n$  and  $f_f$  among the sharers at the cost of redundantly computing a shared bubble by all the sharers. *Fronts* containing the shared portion of the bubble redundantly perform the computations for the shared bubble. Responsibilities of sharers include

solving the equations, keeping track of new sharers, communication with their corresponding *Domains* and sending or receiving the shared data  $x_f$  to or from the sharers. The owner of the shared bubble has the same responsibilities as the sharer with an additional responsibility of sending entire data of the shared bubble to the new sharers.

We analyze these two approaches in terms of their communication overhead and present their implementation in the following sections.

## Modeling Communication

Parallelization of both the Lagrangian and Eulerian grids introduce three types of communication: 1) *Front-Domain*, 2) *Domain-Domain* and 3) *Front-Front*. In this section, we analytically compute message sizes and number of messages sent by each *Front* and *Domain* processes. For the sake of simplicity we assume that the Eulerian grid size is  $N$  in  $x$ ,  $y$  and  $z$  dimensions.

### Front to Domain Communication

The message size in *Front to Domain* communication is variable as it depends on the number of bubbles, deformation in bubbles and the allowed distance between two points of a bubble. The total number of points in the  $i$ th bubble,  $P_i$ , can be approximately given by

$$P_i = \left( \pi r \times \frac{N}{L} \times \frac{1}{\sqrt{a_{min} \times a_{max}}} \right)^2, \quad (14)$$

where  $r$  is the radius of the bubble and  $\frac{N}{L}$  is the ratio of grid size to the length of physical domain.  $a_{min}$  and  $a_{max}$  are the minimum and maximum limits, respectively, for the distance allowed between two points in an element. The total message size between a *Front* and all its *Domains* in a single timestep, denoted by  $M_{f2d}$ , can be computed by

$$M_{f2d} = M_{send} + M_{recv},$$

$$M_{send} = 9 \times \sum_{i=1}^n P_i, \quad M_{recv} = 3 \times \sum_{i=1}^n P_i, \quad (15)$$

where  $M_{send}$  is the data sent and  $M_{recv}$  is the data received by the *Front*. For each point there are point coordinates in  $x$ ,  $y$  and  $z$  directions and every point coordinate has a corresponding surface tension force and normal vector to the edge of element. A total of 9 double precision elements per point should be sent to a *Domain* while only updated point coordinates (3 double precision elements) are received from a *Domain*. Let  $d_x$ ,  $d_y$  and  $d_z$  be the geometry of MPI processes for *Domains*. For the sake of simplicity if we assume  $d = d_x = d_y = d_z$ , then there are  $d^3$  *Domains* in total. The number of messages sent and received by the *Front* in a single timestep would be  $2d^3$  because all point coordinates destined to a single *Domain* could be packed in a single message.

If there are  $f$  *Fronts* and approximately equal number of *Domains* are assigned to each *Front*, then the number of messages and message size per *Front* are reduced by a factor of  $f$ ; each *Front* exchanges  $2d^3/f$  messages with size of

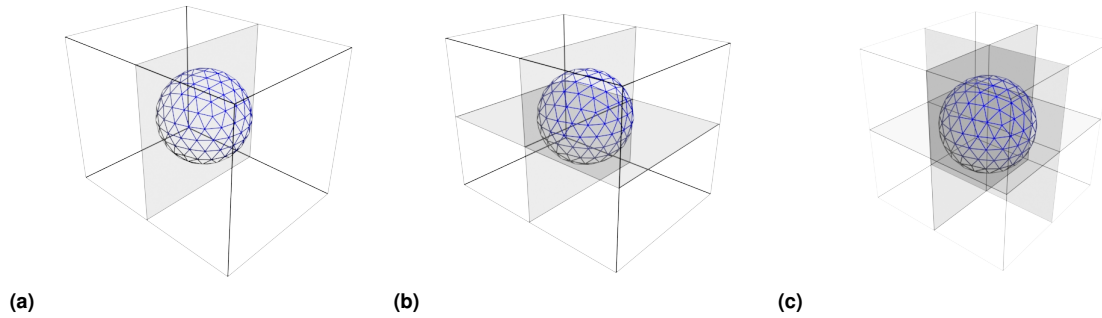


**Figure 4.** Three types of *Front* boundaries: (a) plane boundary - represented by the gray plane, dividing the bubble into two parts, (b) line boundary - is the line where two planes intersect each other and (c) point boundary - is the point where all three planes intersect.

$M_{f2d}/f$ . However, the actual message size per *Front* can vary based on how bubbles are distributed in the physical domain.

### Domain to Domain Communication

The message size in this type of communication is fixed and depends on the stationary Eulerian grid size. Every *Domain* needs to exchange its ghost cells (halos) with its 6 neighbors in  $x$ ,  $y$  and  $z$  directions. Each message size is  $n_g \times \frac{N^2}{d^2}$ , where  $n_g$  is the depth of ghost cells and the subdomain size is  $\frac{N}{d}$ . Thus the *Domain to Domain* communication size,  $M_{d2d}$ , is given by

$$M_{d2d} = 6 \times d \times N^2 \times (n_g \times 14). \quad (16)$$

Each *Domain* needs to send at least 30 messages per timestep. The details are as follows: After receiving of  $n$  and  $f_f$  from the *Front*, these values are interpolated on the Eulerian grid and needed to be updated on the neighboring *Domains*. As every *Domain* communicates with its six neighbors, a total of 6 messages are sent. Ghost cells of flow velocity,  $u$ , are communicated with all six neighboring *Domains* after their computation in Eq. 10 and Eq. 12, resulting in another 12 messages. Pressure and density computed in Eq. 11 and Eq. 4 result in two more message exchanges with six neighbors.

### Front to Front Communication

*Front to Front* communication is required to exchange the point coordinates of the shared bubbles, which were updated by *Domains*. *Front to Front* communication is difficult to approximate as it depends on the number of the shared bubbles, the number of *Fronts* sharing those bubbles and the shared portion of a bubble. Let's suppose that we have  $b$  number of shared bubbles, where each bubble is shared by  $s$  number of *Fronts*. The value of  $b$  depends on the total number of *Fronts* and the movement of bubbles during simulation. There are three types of boundaries between *Fronts* as shown in Fig 4: (1) A plane boundary that is between two adjacent *Fronts*, (2) a line boundary where four neighboring *Fronts* meet, and (3) a point boundary that is shared by eight neighboring *Fronts*.

The probability that a bubble is shared on a certain boundary depends on many variables e.g. the bubble

diameter i.e. if a single large bubble is simulated it is expected to be shared on a point boundary. However here only the probabilities of the boundary types are compared. Probabilities of boundary types are based on the amount of space they occupy in the domain. For example if a domain is divided into 8 subdomains, then there will be only single point boundary, two line boundaries and three plane boundaries. If there are 100 bubbles then at maximum only one bubble can be shared on the point boundary. On the other hand, bubbles shared on the lines are more probable than point and the maximum probability is to be shared on a plane boundary. Moreover the many bubble case is considered here so the diameters of the bubbles are expected to be smaller as compared to the domain size. Thus it is more likely that a bubble will be shared on a plane boundary compared to a line or point. As a result, the value of  $s$  for a large number of shared bubbles is 2.

*Owner-Computes the Shared Bubble Strategy:* In the *owner-computes* strategy the owner of the bubble sends point coordinates, corresponding surface tension force and normal vector to the sharers and then receives the updated point coordinates from them. The amount of shared points is initially small when a bubble becomes shared and increases as the bubble moves. The amount of shared points starts decreasing when a bubble's center crosses the boundary and the ownership is transferred to the neighboring *Front*. In one extreme case (when the center of the bubble is almost at the boundary) fraction of points in the owner *Front* will be slightly more than half, quarter and one eighth of total points for plane, line and point boundaries, respectively. Thus,  $\frac{(s-1)}{s}$  fraction of the points are exchanged with sharers. In another extreme case, only 1 point from each shared bubble is exchanged. Then, the number of messages exchanged per timestep is  $2(s-1)b$ . The minimum and maximum communication size denoted by  $M_{f2fOC_{min}}$  and  $M_{f2fOC_{max}}$ , respectively, for both sending and receiving the point coordinates per timestep driven from Eq. (15) for all the *Fronts* are represented by

$$\begin{aligned} M_{f2fOC_{max}} &= (9+3) \frac{(s-1) \sum_{i=1}^b P_i}{s}, \\ M_{f2fOC_{min}} &= (9+3) \frac{(s-1)b}{s}. \end{aligned} \quad (17)$$

Communication Type	Number of Messages	Communication Size
<i>Front to Domain</i>	$2d^3$	$M_{f2d} = (9 + 3)\sum_{i=1}^n P_i$
<i>Domain to Domain</i>	$30d^3$	$M_{d2d} = 6 \times d \times N^2 \times (n_g \times 14)$
<i>Front to Front</i> (Owner-Computes)	$2(s - 1)b$	$M_{f2fOC_{max}} = (9 + 3)\frac{(s-1)\sum_{i=1}^b P_i}{s}$
(Redundantly-all-Compute)	$s(s - 1)b$	$M_{f2fRC} = (3 \times (s - 1))\sum_{i=1}^b P_i$

**Table 1.** Number of messages and message sizes for different types of communication with the assumption of uniform distribution of bubbles.

*Redundantly-all-Compute the Shared Bubble Strategy:* Communication in *redundantly-all-compute* strategy is different as compared to the *owner-computes* strategy because communication has to take place among all the *Fronts* sharing the bubble and each *Front* has to redundantly send the same point coordinates that were updated in *Front* to all other sharers. The number of messages exchanged per timestep is  $s(s - 1)b$ . The communication size per timestep for all the *Fronts*,  $M_{f2fRC}$ , is given by

$$M_{f2fRC} = (3 \times (s - 1))\sum_{i=1}^b P_i. \quad (18)$$

### Comparison of Communication Overheads

Table 1 summarises the communication overhead for all three types of communication. The number of *Domain* processes ( $d^3$ ) and bubbles ( $n$ ) are dominant factors in the communication overhead. In the simulation the number of shared bubbles,  $b$ , is typically much smaller than the total number of bubbles. Similarly, the number of sharers is smaller than the number of fronts,  $f$  or domains,  $d^3$ . As a result, it is expected that the communication size in *Domain to Domain* is much larger than *Front to Domain*, which is also larger than the *Front to Front* communication. The number of messages is expected to be the highest for *Domain to Domain*. In *Front to Front*, the number of messages mainly depends on how many bubbles are shared and the number of sharers.

The cost model for the *redundantly-all-compute* strategy holds at all times because the model is independent of what portion of a bubble is shared. On the contrary we can only approximate the communication cost of the *owner-computes* strategy. If we take the average of the minimum and maximum communication size into account for *owner-computes*, then the following observations can be made:

- If a bubble is shared at a plane boundary or line boundary, then *redundantly-all-compute* is advantageous in terms of communication size; *owner-computes* strategy would exchange  $3b$  and  $9b$  more double precision elements, for planes and lines respectively.
- If a bubble is shared at a point boundary, then *owner-compute* is advantageous in terms of communication size because there are eight sharers.
- The number of messages for both strategies are equal when a bubble is shared on a plane boundary but *redundantly-all-compute* strategy exchanges more messages when a bubble is shared on a line or a point boundary.

- Considering that it is more likely for bubbles to be shared at a plane or line boundary, *redundantly-all-compute* should perform better because of its smaller overall communication volume. On the other hand, *redundantly-all-compute* comes at the expense of increased computation at the sharer *Fronts*.

Based on these observations, there is no clear winner. The best strategy depends on how the bubbles are shared, the balance between the interconnection network and compute capabilities of the underlying machine, and finally how much communication overhead is hidden behind computation. As a result, it is worthwhile to implement both strategies and explore their actual performance.

### Implementation

The Eulerian grid is partitioned in all three dimensions in space resulting in a number of subgrids (*Domains*), each of which is executed by a separate MPI process. Every *Domain* works on its portion of the stationary Eulerian grid while exchanging boundary values with neighboring *Domains*. The *Domain* processes are responsible for solving the equations on the Eulerian grid indicated in Fig 2. The Poisson equation for the pressure (Eq. 11), and the indicator function (Eq. 13) are solved using the HYPRE library [35].

The interpolation of  $n$  and  $f_f$  from the Lagrangian to Eulerian grid and the interpolation of  $u$  from the Eulerian to Lagrangian grid mentioned in Fig 2 can be done either in the *Domain* or in the *Front* processes. Both these interpolations are done in the *Domain* to reduce the communication size because the Eulerian grid is denser than the Lagrangian grid. We send  $x_f$  from the *Front* to the *Domain* because it is needed for interpolation. The *Domain* process also solves Eq. 8 as it simply updates  $x_f$ .

In the remainder of this section we present the implementation details for the two parallelization strategies for the Lagrangian grid. It is important to note that we use non-blocking communication calls as much as possible as a result some of the communication cost might be hidden behind computation.

#### Parallel Front with Owner-Computes Shared Bubbles

The design for the parallel *Front* using the *owner-computes* strategy is shown in Fig 5a. The inner do-loop executes twice for each timestep to achieve second order accuracy in time. A bubble created initially inside a *Front* may also be shared with another *Front* or it may become shared in any timestep. We implement the *Find\_Shared\_Interface* subroutine, which iterates over all bubbles and finds the bubbles that are shared

```

1 do each timestep
2   Receive_timestep()           !from Domain
3   Store_Previous_Point_Coordinates()
4   do (2 times)
5     Calculate(n, ff)           !Solve Eqn(7)
6     Find_Shared_Interface()
7     Find_Fronts_to_Communicate()
8     Exchange(n, ff, xf)       !with Sharer Fronts
9     Send(n, ff, xf)           !to Domains
10    Receive(xf)                 !from Domains
11    Exchange(xf)                 !with Sharer Fronts
12  end do
13  Calculate_Ave_Point_Coordinates()
14  Regrid_Interface()
15  Calculate_Statistics()
16  Exchange_Interface_Properties() !with Fronts
17  Ownership_Transfer()           ! to the new owner
18 end do

```

(a)

```

1 do each timestep
2   Receive_timestep()           !from Domain
3   Store_Previous_Point_Coordinates()
4   do (2 times)
5     Calculate(n, ff)           !Solve Eqn(7)
6     Send(n, ff, xf)           !to Domains
7     Receive(xf)                 !from Domains
8     Exchange(xf)                 !with Sharer Fronts
9     Find_Shared_Interface()
10    Find_New_Fronts_and_Communicate()
11  end do
12  Calculate_Ave_Point_Coordinates()
13  Regrid_Interface()
14  Calculate_Statistics()
15  Exchange_Interface_Properties() !with Fronts
16  Ownership_Transfer()           !to the new owner
17  Find_Shared_Interface()
18  Find_New_Fronts_and_Communicate()
19 end do

```

(b)

**Figure 5.** (a) Parallel *Front* design of *owner-computes* strategy for the shared bubble. (b) Parallel *Front* design of *redundantly-all-compute* strategy for the shared bubble.

among multiple *Fronts*. The next step is to send and receive the  $n$  and  $f_f$  at the shared point coordinates along with  $x_f$  to and from the sharers.

Instead of all *Fronts* communicating with each other we optimize the communication overhead by adding the *Find\_Fronts\_to\_Communicate* subroutine, which finds and notifies only those *Fronts* that need to communicate with each other. In this subroutine each *Front* fills an array, having length equal to the number of *Fronts*, with a flag to indicate whether it needs to communicate with a specific *Front* or not. A communication table at each *Front* process is built using this array and serves as an input to the *MPI\_AllGather*. Based on this communication table all owners exchange  $n, f_f$  and  $x_f$  with sharers in the *Exchange*( $n, f_f, x_f$ ) subroutine and then all *Fronts* communicate with their corresponding *Domains*. After receiving the updated point coordinates  $x_f$  from *Domains*, sharers in the *Exchange*( $x_f$ ) subroutine send these updated point coordinates to the owners.

In the *Exchange\_Interface\_Properties* subroutine a single *Front* gather *Interface\_Properties* for all bubbles from their owners and then broadcasts these to all *Fronts*. At the end of a timestep if the center of the bubble has moved from the owner *Front* to some other *Front* then the ownership is transferred to the new *Front*. When that happens, the *Ownership\_Transfer* subroutine sends all the point coordinates, element corners, neighbors and surface tension data to the new owner.

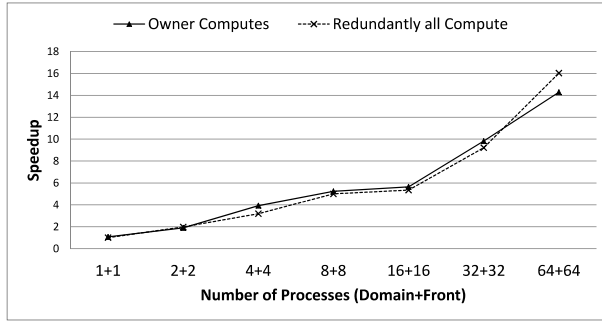
## Parallel Front with Redundantly-All-Compute Shared Bubbles

Fig 5b shows the design for the *redundantly-all-compute* strategy. During the initialization every *Front* performs additional work to find the shared bubbles and notifies the sharers to redundantly create that bubble. After creating the shared bubbles redundantly each *Front* calculates surface tension force and normal vectors at the corresponding point coordinates and sends them to their allocated *Domains*. After receiving the updated point coordinates  $x_f$  from the *Domains*, each *Front* in the *Exchange*( $x_f$ ) subroutine send its received portion of the point coordinates to all other sharers so that every *Front* can have all the relevant point coordinates for the shared bubbles.

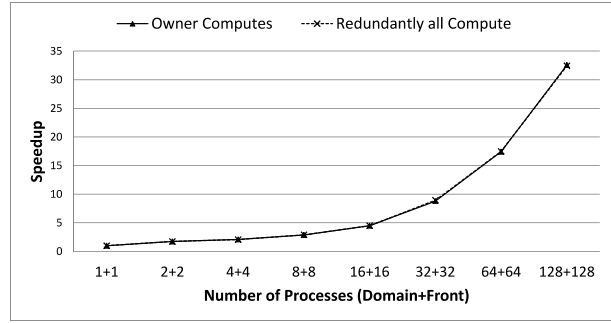
As a result of the point coordinate update and movement of a bubble, some portion of a bubble may now be shared with a new *Front* that was previously not computing the bubble. The *Find\_Shared\_Interface* subroutine is called to find the shared bubbles and their sharers. Subsequently in the *Find\_New\_Fronts\_and\_Communicate* subroutine the owner of the bubbles finds the new sharers and send them all the point coordinates, old point coordinates, element corners, neighbors and surface tension so that these new sharers can redundantly start computing the shared bubble. *Exchange\_Interface\_Properties* works similar to the one in *owner-computes* strategy. However in the *Ownership\_Transfer* subroutine sending bubble's data is eliminated because all the *Fronts* sharing the bubble have already computed that information. Lastly, because averaging and regridding subroutines may introduce new sharers, *Find\_Shared\_Interface* and *Find\_New\_Fronts\_and\_Communicate* functions are called again to discover new sharers.

## Results and Discussion

We carry out the performance studies for the parallel front tracking method on two supercomputers. The first one is the Abel cluster located at the University of Oslo and other is the Hazel Hen located at the High Performance Computing Centre, Stuttgart. Specifications of both Abel and Hazel Hen are listed in Table 2. Abel has an FDR Infiniband interconnection network while Hazel Hen has a Cray Aries Dragonfly network. Throughout the performance studies we use 0.058 void fraction and deformable bubbles with fluid properties given in Table 3. Fluid properties are mainly based on the deformable bubble case used by Lu and Tryggvason [36] and the bubble's diameter is selected so that a bubble can have a reasonable number of grid points i.e., 28 in this case. We use periodic boundary conditions for all directions and double precision arithmetic in our calculations. In our experiments we found that shared memory parallelism do not perform well as compared to distributed memory parallelism. Using hyper-threading within MPI processes produces optimal performance. This conclusion is aligned with prior work by Regulý et al. [37]. All our experiments use 2 OpenMP threads for hyper-threading within each MPI process.



(a) Abel



(b) Hazel Hen

Figure 6. Strong scaling speedup. (higher is better)

Machine Name	Abel	Hazel Hen
CPUs	Intel E5-2670 Sandy Bridge [38]	Intel E5-2680 v3 Haswell [39]
Sockets / Cores per socket	2 / 8	2 / 12
Threads per core	2	2
Clock Rate (GHz)	2.6	2.5
Shared L3 (MB)	20	30
Main memory (GB)	64	128
Memory bandwidth	58 (GB/s)	68 (GB/s)
Network bandwidth	6.78 (GB/s)	11.7 (GB/s)

Table 2. Machine specifications for Abel and Hazel Hen

Bubble diameter ( $d_b$ )	0.16/0.08
Bubble/fluid density ( $\rho_b/\rho_f$ )	0.1/1.0
Bubble/fluid viscosity ( $\mu_b/\mu_f$ )	0.0003333/0.0003333
Surface tension ( $\sigma$ )	0.002
Eotvos number ( $\Delta\rho g d_b^2/\sigma$ )	3.0
Morton number ( $\Delta\rho g \mu_f^4/\rho_f^2 \sigma^3$ )	$3.6155 \times 10^{-7}$

Table 3. Fluid properties

Domain size (x, y, and z)	$2 \times 2 \times 2$
Mesh resolution	$256 \times 256 \times 256$ (Abel) / $512 \times 512 \times 512$ (Hazel Hen)
Number of bubbles	216 (Abel) / 1728 (Hazel Hen)
Number of processes (x,y,z) = Domain process geometry + Front process geometry	$2 = 1 \times 1 \times 1 + 1 \times 1 \times 1$ $4 = 2 \times 1 \times 1 + 2 \times 1 \times 1$ $8 = 2 \times 2 \times 1 + 2 \times 2 \times 1$ $16 = 2 \times 2 \times 2 + 2 \times 2 \times 2$ $32 = 4 \times 2 \times 2 + 4 \times 2 \times 2$ $64 = 4 \times 4 \times 2 + 4 \times 4 \times 2$ $128 = 4 \times 4 \times 4 + 4 \times 4 \times 4$ $256 = 8 \times 4 \times 4 + 8 \times 4 \times 4$ $512 = 8 \times 8 \times 4 + 8 \times 8 \times 4$
MPI processes/node	16 (Abel) / 24 (Hazel Hen)

Table 4. Strong scaling inputs.

### Strong Scaling

Strong scaling studies enable us to observe the behavior of the code for solving the same problem with more resources. Grid parameters and different input configurations for strong scaling runs are given in Table 4. Domain size is the container size that we are simulating and mesh resolution is the Eulerian grid that is used in the *Domain*. Baseline for the speedup is the *redundantly-all-compute* strategy with two MPI processes one for the *Domain* and one for the *Front*.

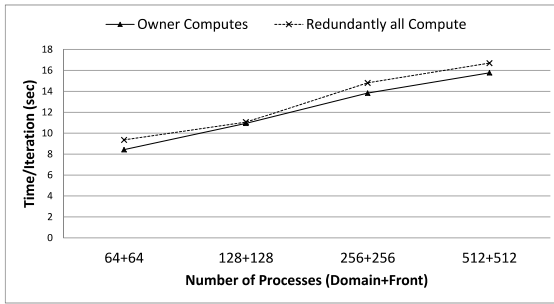
Fig 6 shows the results for the strong scaling. On Abel, for the given mesh size ( $256^3$ ), the best speedup for both strategies is achieved when 64 *Domain* + 64 *Front* processes are used. The speedup over the baseline with 1+1 processes

is 16x for *redundantly-all-compute* and 14x for *owner-computes* strategy. Increasing MPI processes beyond 128 not realistic because at that point there are only few data points assigned to each MPI process. On Hazel Hen, we achieve much better scalability because Hazel Hen has a higher network bandwidth, which is 11.7 GB/s, almost twice of that of Abel. The maximum speedup we achieve on Hazel Hen is around 32.5x over 1+1 processes for both strategies. Again here increasing the MPI processes beyond 256 is not realistic.

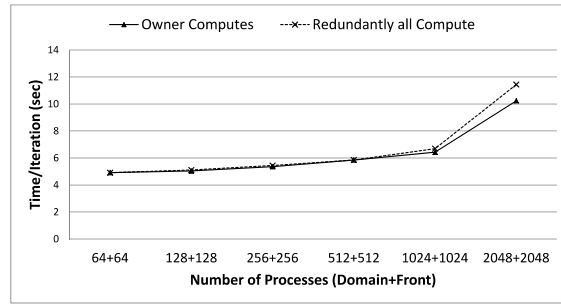
When we compare two parallelization strategies of the Lagrangian grid, the *redundantly-all-compute* strategy performs better than the *owner-computes* strategy when the number of processes are large. This is because increasing the number of processes results in more subdomains, thus more boundaries ultimately increasing the number of shared bubbles. For fewer number of processes *owner-computes* performs better because the communication overhead due to shared bubbles is lower than the extra computation performed by the *redundantly-all-compute* strategy. These results are in line with our conclusions in communication modeling i.e. the communication overhead due to shared bubble is lower for *redundantly-all-compute* strategy at the expense of extra computation. The performance gap between the two strategies is small, not visible in the figure, on Hazel Hen as compared to Abel due to the fast interconnection network on Hazel Hen.

	Input-1/2/3/4/5/6
Domain size (x, y, z)	$2 \times 4 \times 4/4 \times 4 \times 4/$ $4 \times 8 \times 4/4 \times 8 \times 8/$ $8 \times 8 \times 8/8 \times 8 \times 16$
Mesh resolution	$256 \times 512 \times 512/$ $512 \times 512 \times 512/$ $512 \times 1024 \times 512/$ $512 \times 1024 \times 1024/$ $1024 \times 1024 \times 1024/$ $1024 \times 1024 \times 2048$
Number of bubbles	$864/1728/3456/$ $6912/13824/27648$
Number of processes (x,y, z) = Domain process geometry + Front process geometry	$128 = 4 \times 4 \times 4 + 4 \times 4 \times 4/$ $256 = 8 \times 4 \times 4 + 8 \times 4 \times 4/$ $512 = 8 \times 8 \times 4 + 8 \times 8 \times 4/$ $1024 = 8 \times 8 \times 8 + 8 \times 8 \times 8$ $2048 = 8 \times 8 \times 16 + 8 \times 8 \times 16$ $4096 = 8 \times 16 \times 16 + 8 \times 16 \times 16$
MPI processes/node	16 (Abel) / 24 (Hazel Hen)

Table 5. Weak scaling inputs.



(a) Abel



(b) Hazel Hen

Figure 7. Weak scaling. (lower is better)

### Weak Scaling

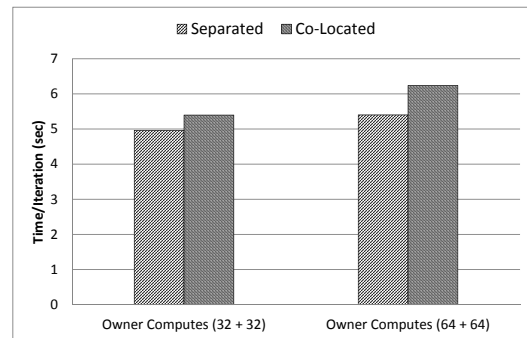
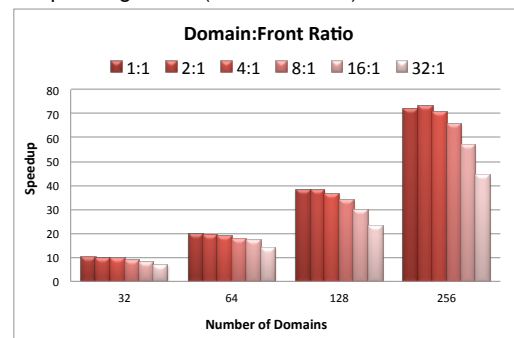
We conduct weak scaling study for the front tracking method because high mesh resolutions allow researchers to investigate complex fluid-fluid or fluid-gas interaction problems. Inputs for weak scaling are shown in Table 5. In this study, we fix the amount of computational work assigned to each process in all six inputs :  $64 \times 128 \times 128$  grid size to each *Domain* process, and approximately 14 bubbles to each *Front* process.

Results for weak scaling are shown in Fig 7. Although the computational work per process stays the same, the time per iteration slowly rises as we scale due to the communication overhead on Abel. On the other hand both strategies show good scaling on Hazel Hen up to 2048 processes (1024+1024) but time per iteration rises with further increase in the number of processes. Although the number of messages and communication size per process stay the same, the total number of messages and message sizes increase in all three types of communication that leads to network contention. In the implementation we use global synchronizations such as *MPI\_AllReduce* to select minimum timestep value, *MPI\_AllGather* to assemble communication matrix in the *Front* processes, and *MPI\_Broadcast* to send interface properties to the *Front* processes. These global synchronizations lowers the parallel efficiency beyond 2048 processes. Future work will further improve the communication and synchronization costs by removing some of the global synchronisation points.

### Process Placement and Ratios

We also compare two placement scenarios for the *Domain* and *Front* processes. In the first scenario, ‘co-located’, *Domains* and their corresponding *Fronts* are placed in the same compute node while in the second scenario, ‘separated’, *Domains* and *Fronts* processes are placed in separate compute nodes. For example, consider the case of 8 (4+4), where processes numbered 0-3 are the *Domain* processes and 4-7 are the *Front* processes. In the separated scenario we schedule the processes 0-3 to run on the first node and 4-7 on the second node. In the co-located scenario processes 0,2,4,6 are scheduled to run on the first node and 1,3,5,7 on the second node. Note that in both scenarios the same number of resources (cores and nodes) are used to schedule MPI processes. We use “cyclic:cyclic” for co-located and “block:block”

for separated in the SLURM [40] task distribution method in the job submission script. As shown in Fig 8 placing *Fronts* and their corresponding *Domains* in separated nodes performs better than co-locating them in the same node. The performance improvement becomes clearer as the number of processes is increased. Indeed our communication model suggests that the separated task distribution should perform better because the *Domain* to *Domain* communication plus *Front* to *Front* communication is more than the *Front* to *Domain* communication. For example, consider the (32+32) case. Based on Eq. (15-17), in a single timestep, *Domain* to *Domain* communication results in 36.7MB of data exchange in 960 messages, *Front* to *Front* communication results in 5.77MB of data exchange using 216 messages, and finally *Front* to *Domain* communication results in 34.6MB of data exchange in 64 messages. As a result, placing these two types of processes on different nodes is the best since node to node communication is more costly than within the node communication.

Figure 8. Co-located vs separated *Domain* and corresponding *Front*. (lower is better)Figure 9. Number of *Domains* to number of *Fronts* ratio (higher is better)

In Fig 6 we ran the application by assigning one *Front* to every *Domain*. Next, we experiment with different *Domain* to *Front* ratios to find an optimal value. The ratio between *Domain* and *Front* processes should be balanced to avoid underutilization of resources. Computation performed by a *Front* process is considerably less expensive than a *Domain* process. Thus sparing more processes for *Front* than *Domain* is not beneficial. The result shown in Fig 9 suggests that assigning single *Front* to every 4 *Domains* can achieve almost the same speedup as single *Front* to single *Domain*. 2:1 ratio (two *Domains* for every *Front*) performs slightly better in some cases, however in strong and weak scaling we did not observe any significant gain for 2:1 ratio over 1:1 because the benefit of additional resources is negated by the additional communication overhead. Although the figure shows only *owner-computes* strategy, the *Domain* to *Front* ratios for both strategies give similar performance.

## Conclusions

Eulerian-Lagrangian methods for multiphase flows simulations are more challenging than Eulerian methods to parallelize because the Lagrangian grid is unstructured, movable, restructures continuously with time and requires coupling with the Eulerian grid. In this work, we focused on the parallelization of front tracking method that belongs to the family of the Eulerian-Lagrangian approach. The parallelization of the method is necessary to be able to simulate large number of interfaces (bubbles) and to overcome the memory limitation on a single compute node. We implemented and analysed two different parallelization strategies for the Lagrangian grid, namely *owner-computes* and *redundantly-all-compute*. The communication cost model we devised for these parallelization strategies suggests that the best performing strategy depends on the distribution of bubbles in the fluid and the underlying machine specifications.

Our implementation can achieve 32.5x speedup on 256 cores on the Hazel Hen supercomputer and 16x speedup on the Abel supercomputer with 128 cores over the baseline (2 cores) with strong scaling. We conduct the weak scaling study of our code by simulating up to 28 thousand bubbles on  $1024 \times 1024 \times 2048$  grid size using about four thousand cores, and achieve very good scaling. The experimental results indicate that *owner-computes* slightly performs better on weak scaling studies but *redundantly-all-compute* performs better in strong scaling studies. Thus, we expect that on a machine with high compute capability but low network bandwidth, *redundantly-all-compute* is likely to outperform *owner-computes*. Finally co-locating *Domain* processes on the same node performs better than splitting a node between *Domain* and its corresponding *Front* processes because the *Domain* to *Domain* communication size is significantly more than the *Front* to *Domain* communication.

## Acknowledgments

This research is supported by the Turkish Science and Technology Research Centre Grant No: 215E193. We acknowledge PRACE for awarding us access to the Hazel Hen supercomputer in Germany. Lastly we thank Xing Cai from Simula Research Laboratory for his input.

## References

- [1] Deckwer WD (1992) *Bubble Column Reactors*. Wiley.
- [2] Furusaki S, Fan LS and Garside J (2001) *The expanding world of chemical engineering*, 2nd ed. London: Taylor and Francis.
- [3] Tryggvason G, Scardovelli R and Zaleski S (2011) *Direct numerical simulations of gas-liquid multiphase flows*. Cambridge University Press.
- [4] Alfonsi G, Ciliberti SA, Mancini M and Primavera L (2014) GPGPU implementation of mixed spectral-finite difference computational code for the numerical integration of the three-dimensional time-dependent incompressible Navier-Stokes equations. *Computers & Fluids*, 102:237-249.
- [5] Aggarwal V, Gada VH and Sharma A (2013) Parallelization methodology and performance study for level set method based simulation of a 3-D transient two-phase flow. *Numer. Heat Transfer, B*, 63:327-356.
- [6] Bunner B (2000) *Large scale simulations of bubbly flow*. PhD Thesis. University of Michigan.
- [7] Reddy R and Banerjee R (2015) GPU accelerated VOF based multiphase flow solver and its application to sprays. *Computers & Fluids*, 117:287-303.
- [8] Li XL (1993) Study of three-dimensional Rayleigh-Taylor instability in compressible fluids through level set method and parallel computation. *Physics of Fluids*, 5:1904;
- [9] George WL and Warren JA (2002) A parallel 3D dendritic growth simulator using the phase-field method. *Journal of Computational Physics*, 177:264-283.
- [10] Wang K, Chang A, Kale LV and Dantzig JA (2006) Parallelization of a level set method for simulating dendritic growth. *Journal of Parallel and Distributed Computing*, 66:1379-1386.
- [11] Nkonga B and Charrier P (2002) Generalized parcel method for dispersed spray and message passing strategy on unstructured meshes. *Parallel Computing*, 28:369-398.
- [12] Darmana D, Deen NG and Kuipers JAM (2006) Parallelization of an Euler-Lagrange model using mixed domain decomposition and a mirror domain technique: application to dispersed gas-liquid two-phase flow. *Journal of Computational Physics*, 220:216-248.
- [13] Kuan CK, Sim J, Hassan E and Shyy W (2013) Parallel Eulerian-Lagrangian Method with Adaptive Mesh Refinement for Moving Boundary Computation. In: *51st AIAA Aerospace Sciences Meeting including the New Horizons Forum and Aerospace Exposition, Aerospace Sciences Meetings*, Grapevine, Texas, 7-11 January 2013.
- [14] Glimm J, Grove J, Lindquist B, McBryan O and G. Tryggvason (1988) The bifurcation of tracked scalar waves. *SIAM J. Sci. Stat. Comput.*, 9(1):61-79.
- [15] Glimm J, Grove JW, Li XL, Oh W and Sharp DH (2001) A critical analysis of Rayleigh-Taylor growth rates. *Journal of Computational Physics*, 169:652-677.
- [16] Glimm J, Grove JW, Li XL and Tan DC (2000) Robust computational algorithms for dynamic interface tracking in three dimensions. *SIAM J. Sci. Comput.*, 21(6):2240-2256.
- [17] Glimm J, Grove JW and Zhang Y (2002) Interface tracking for axisymmetric flows. *SIAM J. Sci. Comput.*, 24:208-236.

- [18] Fix B, Glimm J, Li X, Li Y, Liu X, Samulyak R and Xu Z (2005) A TSTT integrated frontier code and its applications in computational fluid physics. *J. Phys.: Conf. Ser.*, 16: 471-475.
- [19] Unverdi SO and Tryggvason G (1992) A front-tracking method for viscous, incompressible, multi-fluid flows. *Journal of Computational Physics*, 100:25-37.
- [20] Tryggvason G, Bunner B, Esmaeeli A, Juric D, Al-Rawahi N, Tauber W, et al. (2001) A front tracking method for the computations of multiphase flow. *Journal of Computational Physics*, 169:708-759.
- [21] Esmaeeli A and Tryggvason G (1996) An inverse energy cascade in two-dimensional, low Reynolds number bubbly flows. *Journal of Fluid Mechanics*, 314:315-330.
- [22] Bunner B and Tryggvason G (2002) Dynamics of homogeneous bubbly flows. Part 1. Rise velocity and microstructure of the bubbles. *Journal of Fluid Mechanics*, 466:17-52.
- [23] Bunner B and Tryggvason G (2002) Dynamics of homogeneous bubbly flows. Part 2. Velocity fluctuations. *Journal of Fluid Mechanics*, 466:53-84.
- [24] Demmel J (2013) Communication-avoiding algorithms for linear algebra and beyond. In: *27th IEEE International Parallel & Distributed Processing Symposium (IPDPS2013)*, Boston, MA, 20-24 May 2013, pp. 585-585.
- [25] You Y, Demmel J, Czechowski K, Song L and Vuduc R (2015) CA-SVM: Communication-Avoiding Support Vector Machines on Distributed Systems. In: *29th IEEE International Parallel & Distributed Processing Symposium (IPDPS2015)*, Hyderabad, India, 25-29 May 2015, pp. 847-859.
- [26] Driscoll M, Georganas E, Koanantakool P, Solomonik E and Yelick K (2013) A Communication-Optimal N-Body Algorithm for Direct Interactions. In: *27th IEEE International Parallel & Distributed Processing Symposium (IPDPS2013)*, Boston, MA, 20-24 May 2013, pp. 1075-1084.
- [27] Leonard BP (1979) A stable and accurate convective modelling procedure based on quadratic upstream interpolation. *Computer Methods in Applied Mechanics and Engineering*, 19(1):59-98.
- [28] Chorin AR (1968) Numerical solution of the Navier-Stokes equations. *Mathematics of Computation*, 22:745-762.
- [29] Peskin CS (1977) Numerical analysis of blood flow in the heart. *Journal of Computational Physics*, 25:220-252.
- [30] Muradoglu M and Tasoglu S (2010) A front tracking method for computational modeling of impact and spreading of viscous droplets on solid walls. *Computers & Fluids*, 39(4):615-625.
- [31] Muradoglu M and Tryggvason G (2014) Simulations of soluble surfactants in 3D multiphase flow. *Journal of Computational Physics*, 274:737-757.
- [32] Izbassarov D and Muradoglu M (2015) A front-tracking method for computational modeling of viscoelastic two-phase systems. *Journal of Non-Newton. Fluid Mechanics*, 223:122-140.
- [33] Terashima H and Tryggvason G (2010) A front tracking method with projected interface conditions for compressible multi-fluid flows. *Computers & Fluids*, 39(10):1804-1814.
- [34] Shin S, Yoon I and Juric D (2011) The local front reconstruction method for direct simulation of two- and three-dimensional multiphase flows. *Journal of Computational Physics*, 230(17):6605-6646.
- [35] HYPRE Library. Lawrence Livermore National Laboratory, Available at: [http://computation.llnl.gov/project/linear\\_solvers/software.php](http://computation.llnl.gov/project/linear_solvers/software.php). (accessed 21 April 2016)
- [36] Lu J and Tryggvason G (2008) Effect of bubble deformability in turbulent bubbly upflow in a vertical channel. *Physics of Fluids*, 20:040701.
- [37] Reguly I, Mudalige D, Bertolli C, Giles M, Betts A, Kelly P, Radford D (2016) Acceleration of a Full-Scale Industrial CFD Application with OP2. *IEEE Transactions on Parallel and Distributed Systems*, 27(5):1265-1278.
- [38] Intel Xeon Processor E5-2670, <http://ark.intel.com/products/64595/Intel-Xeon-Processor-E5-2670-20M-Cache-2.60-GHz-8.00-GTs-Intel-QPI>. (accessed 09 January 2017)
- [39] Intel Xeon Processor E5-2680 v3, <http://ark.intel.com/products/81908/Intel-Xeon-Processor-E5-2680-v3-30M-Cache-2.50-GHz>. (accessed 09 January 2017)
- [40] SLURM. Lawrence Livermore National Laboratory, Available at: <https://computing.llnl.gov/linux/slurm/sbatch.html>. (accessed 21 April 2016)
- [41] Ang J, Barrett R, Benner R, Burke D, Chan C, Cook J, Donofrio D, Hammond S, Hemmert K, Kelly S, Le H, Leung V, Resnick D, Rodrigues A, Shalf J, Stark D, Unat D and Wright N (2014) Abstract Machine Models and Proxy Architectures for Exascale Computing. *Hardware-Software Co-Design for High Performance Computing (Co-HPC)*.
- [42] Unat D, Chan C, Zhang W, Williams S, Bachan J, Bell J, and Shalf J (2015) Exasat: An exascale co-design tool for performance modeling. *International Journal of High Performance Computing Applications*, 29(2):209-232.